### Title

Tunable Cherenkov Radiation of Phonon Polaritons in Silver Nanowire/Hexagonal Boron Nitride Heterostructures




### Journal

Nano Letters, 20(4)

### ISSN

1530-6984



### Authors

Zhang, Yiran
Hu, Cheng
Lyu, Bosai
et al.



### Publication Date

2020-04-08

### DOI

10.1021/acs.nanolett.0c00419

Peer reviewed

NANO LETTERS

pubs.acs.org/NanoLett Letter

# Tunable Cherenkov Radiation of Phonon Polaritons in Silver Nanowire/Hexagonal Boron Nitride Heterostructures

Yiran Zhang,[○] Cheng Hu,[○] Bosai Lyu, Hongyuan Li, Zhe Ying, Lele Wang, Aolin Deng, Xingdong Luo, Qiang Gao, Jiajun Chen, Jing Du, Peiyue Shen, Kenji Watanabe, Takashi Taniguchi, Ji-Hun Kang, Feng Wang, Yueheng Zhang, and Zhiwen Shi*

Cite This: *Nano Lett.* 2020, 20, 2770−2777 Read Online

ACCESS | Metrics & More | Article Recommendations | Supporting Information

**ABSTRACT:** Polaritons in two-dimensional (2D) materials have shown their unique capabilities to concentrate light into deep subwavelength scales. Precise control of the excitation and propagation of 2D polaritons has remained a central challenge for future on-chip nanophotonic devices and circuits. To solve this issue, we exploit Cherenkov radiation, a classic physical phenomenon that occurs when a charged particle moves at a velocity greater than the phase velocity of light in that medium, in low-dimensional material heterostructures. Here, we report an experimental observation of Cherenkov phonon polariton wakes emitted by superluminal one-dimensional plasmon polaritons in a silver nanowire and hexagonal boron nitride heterostructure using near-field infrared nanoscopy. The observed Cherenkov radiation direction and radiation rate exhibit large tunability through varying the excitation frequency. Such tunable Cherenkov phonon polaritons provide opportunities for novel deep subwavelength-scale manipulation of light and nanoscale control of energy flow in low-dimensional material heterostructures.

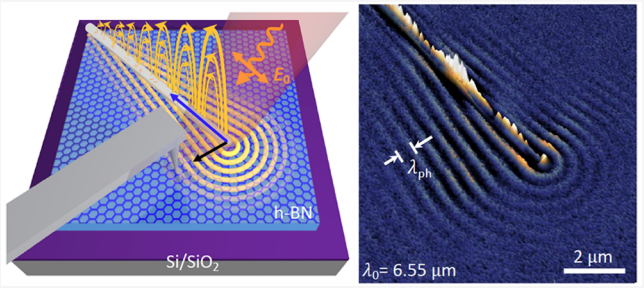


**KEYWORDS:** *Cherenkov radiation, 2D materials, infrared nanoscopy, phonon polaritons*



Low-dimensional material heterostructures assembled from graphene, hexagonal boron nitride (hBN), nanowires and other nanoscale components are an emergent class of material building blocks that have attracted much research interest.[1−11] These heterostructures can exhibit completely new electronic and optical phenomena, such as the emergence of superlattice Dirac points,[1−5] Hofstadter's butterfly,[2−4] tunable Mott insulator,[6,7] unconventional superconductor[8] and moiré excitons,[9−11] which demonstrate that low-dimensional material heterostructures are ideal platforms for exploring novel physics phenomena.

Specifically, in low-dimensional materials, the light−matter interactions endow polaritons with largely reduced phase velocities and strong coupling,[12−19] both of which are key characteristics for Cherenkov radiation. Classic Cherenkov radiation describes the emission of light wakes by a charged particle moving with a speed exceeding the phase velocity of light in that medium. This phenomenon was first experimentally discovered more than 80 years ago by Cherenkov[20] and later theoretically explained by Tamm and Frank,[21] who showed that both the energy and the momentum can be conserved simultaneously in a radiation process for a particle moving at a superluminal speed. Even today, interest in Cherenkov radiation continues, especially in the study of how moving charged particles interact with sophisticated metamaterials and photonic crystals.[22−26] However, generating Cherenkov radiation at the nanometer scale with large tunability remains an outstanding challenge. Realizing Cherenkov radiation in a simple heterostructure of low-dimensional materials, where highly confined polaritons mimic the interaction between a charged particle and dielectric medium, may resolve this issue and provide precise control of polariton launching and propagation as well.

Here, we report experimental observation of Cherenkov radiation of phonon polariton wakes emitted by propagating one-dimensional (1D) plasmon polaritons in a silver nanowire (SNW)/hBN heterostructure using scanning near-field optical microscopy (SNOM). Cherenkov radiation can be switched on and off by tuning the polarization of the excitation laser, which controls the plasmon modes in the SNW. In addition, the Cherenkov angle between the wavefront of phonon polaritons and the SNW is adjustable through varying the excitation

**Received:** February 1, 2020
**Revised:** March 2, 2020
**Published:** March 6, 2020




https://dx.doi.org/10.1021/acs.nanolett.0c00419
*Nano Lett.* 2020, 20, 2770−2777

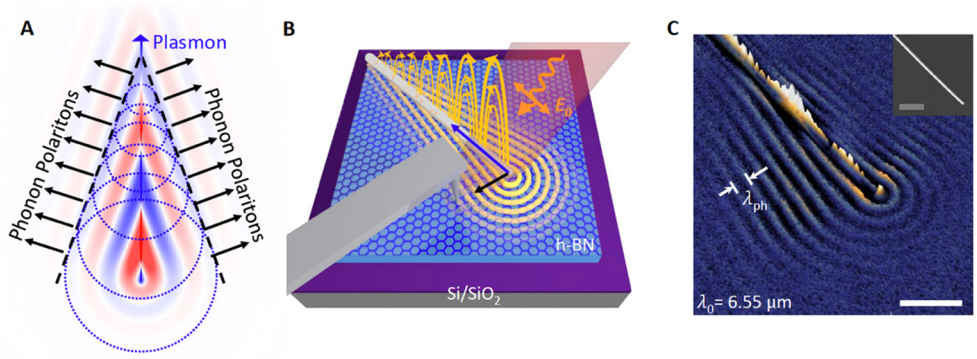


**Figure 1.** Infrared nanoimaging of Cherenkov phonon polaritons in a silver nanowire (SNW) and hexagonal boron nitride (hBN) heterostructure. (A) A schematic diagram of Cherenkov radiation of phonon polaritons from 1D plasmons. (B) Illustration of near-field infrared nanoimaging. The SNW is illuminated by a laser beam with electric field $E_0$ parallel to the nanowire. Such illumination excites longitudinal plasmons at the end of the nanowire. The propagating 1D plasmon generates Cherenkov phonon polariton wakes in hBN. (C) An infrared nanoimage of Cherenkov phonon polaritons at excitation of 6.55 $\mu$m in a typical SNW/hBN heterostructure. The plasmon-launched phonon polariton wavefronts form a nonzero angle relative to the SNW. Inset, AFM topography image of the heterostructure. Scale bars: 2 $\mu$m.

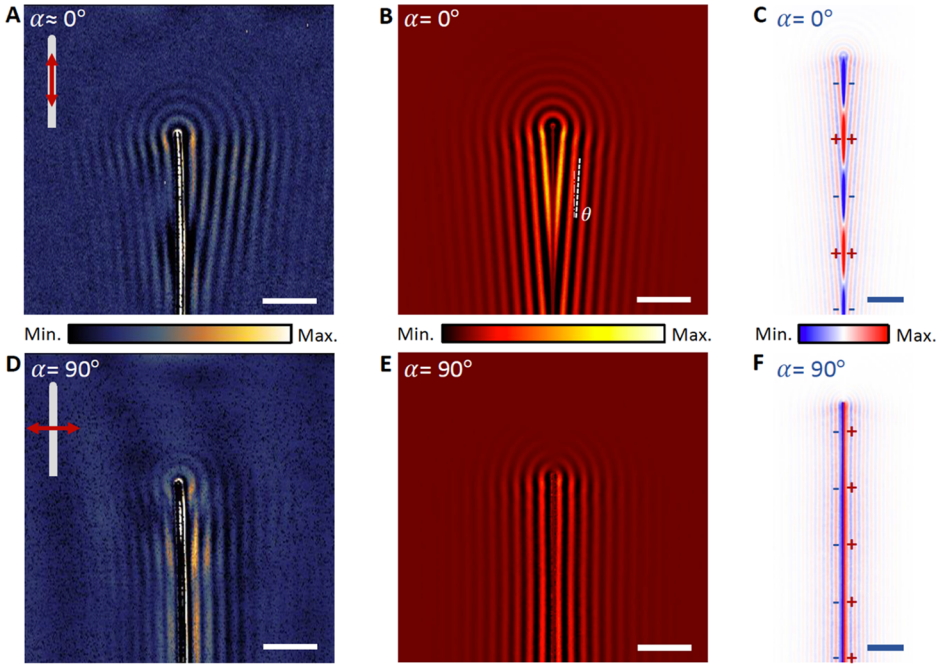


**Figure 2.** Dependence of Cherenkov phonon polaritons on excitation polarization. (A,D) Near-field infrared images of phonon polaritons in an SNW/hBN heterostructure with 6.55 $\mu$m excitation at two representative polarization angles $\alpha \approx 0°$ (A) and 90° (D). The orientations of the phonon polariton wavefronts show large distinctions for the two excitation polarizations. (B,E) Numerical simulations of the near-field distribution of phonon polaritons in the SNW/hBN heterostructure with the excitation light polarized along (B) and perpendicular to (E) the nanowire. (C,F) Simulated corresponding longitudinal (C) and transverse (F) plasmon modes on the SNW. Scale bars: 2 $\mu$m.

wavelength or the thickness of hBN. The observed Cherenkov radiation angle and wavelength agree quantitatively with Cherenkov physics. Moreover, the radiation rate also shows a strong dependence on the excitation wavelength. Thus, Cherenkov radiation with high controllability holds great potential for novel nanophotonic devices requiring polarization- and wavelength-controlled directionality and intensity of light. Furthermore, the observed Cherenkov launching of phonon polaritons offers fundamental insight into the coupling between polaritons of different dimensionalities.

SNWs with diameters ranging from 100 to 150 nm and lengths over 30 $\mu$m in ethanol solutions were spin-coated onto thin hBN flakes on $SiO_2$/Si substrates to create SNW/hBN heterostructures. Direct experimental probe of the Cherenkov phonon polaritons in the SNW/hBN system was provided by infrared nanoimaging via a home-built SNOM setup (see Methods for more details). As shown in Figure 1B, an *s*-polarized single-wavelength laser beam with tunable wavelength from 6.3 to 7.0 $\mu$m was focused onto the end of an SNW. The laser beam direction was perpendicular to the nanowire, and the polarization of the light was parallel to the nanowire. Such illumination excites plasmons at the end of the nanowire, where momentum matching can be fulfilled by the abrupt change of the structure. The excited plasmons propagate longitudinally along the nanowire and couple to the phonon polariton modes in hBN. The plasmon wavelength in SNW is typically much longer than the phonon polariton wavelength in hBN, meaning that the plasmons propagate


https://dx.doi.org/10.1021/acs.nanolett.0c00419
Nano Lett. 2020, 20, 2770−2777

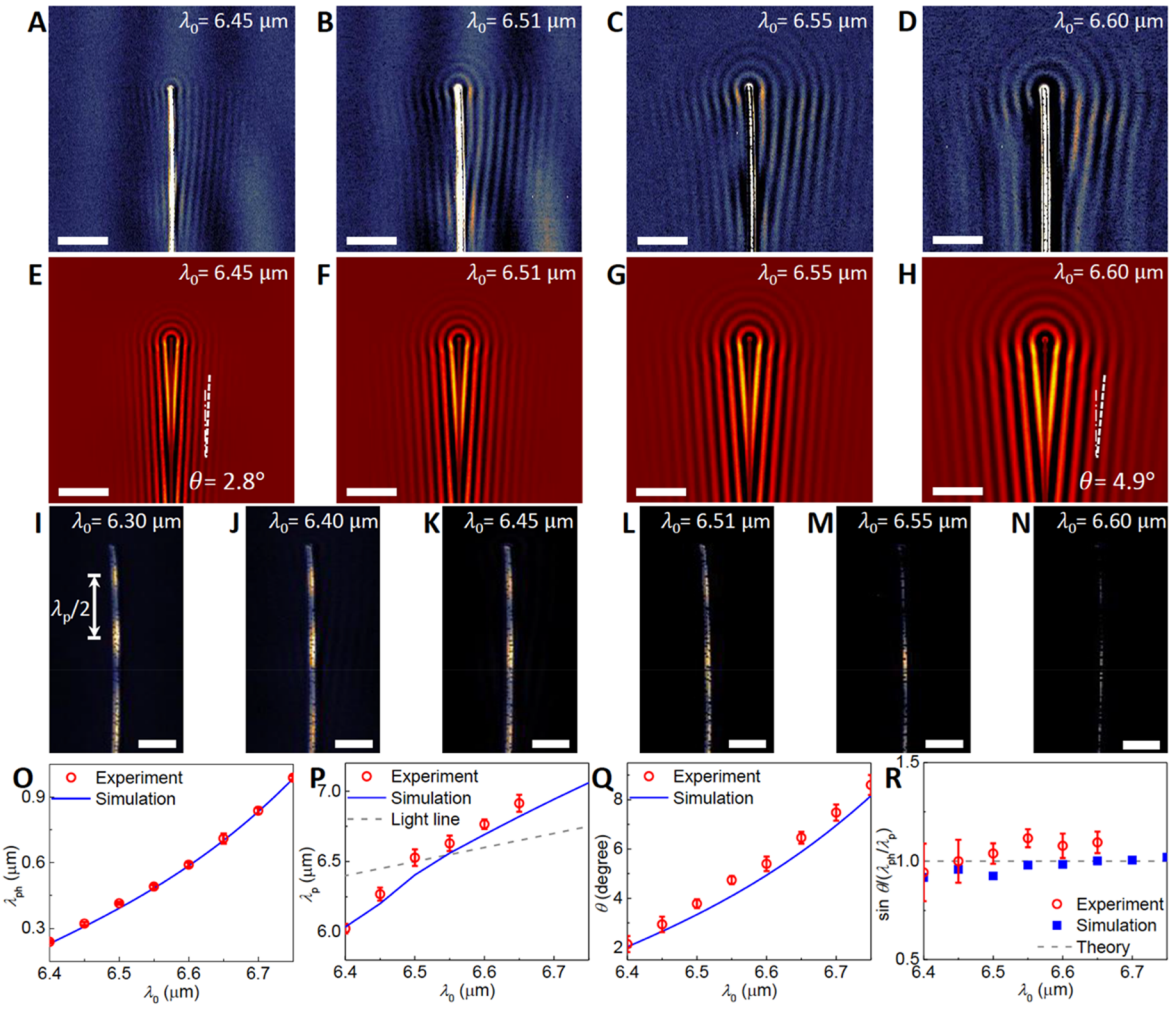


**Figure 3.** Steering of Cherenkov phonon polaritons by varying the excitation wavelength. (A–D) Experimental Cherenkov radiation of phonon polaritons with excitation wavelengths $\lambda_0$ of 6.45 $\mu$m (A), 6.51 $\mu$m (B), 6.55 $\mu$m (C) and 6.60 $\mu$m (D). The Cherenkov angle $\theta$ increases with increasing excitation wavelength $\lambda_0$, as predicted by eq 1. (E–H) Simulated near-field distribution images of the corresponding excitation wavelengths. Scale bars: 2 $\mu$m. (I–N) Plasmon oscillations along the SNW at different excitation wavelengths: 6.30 $\mu$m (I), 6.40 $\mu$m (J), 6.45 $\mu$m (K), 6.51 $\mu$m (L), 6.55 $\mu$m (M), and 6.60 $\mu$m (N). Scale bars: 1 $\mu$m. (O) Experimentally (red circles) and numerically (blue line) obtained dependence of the phonon polariton wavelength on the excitation wavelength. (P) The extracted value of the plasmon wavelength $\lambda_p$ as a function of the excitation wavelength. $\lambda_p$ can sometimes even exceed the free-space photon wavelength $\lambda_0$. (Q) The relation between the Cherenkov angles and the excitation wavelengths. The Cherenkov angle and the phonon polariton wavelength have similar increasing dependence on the excitation wavelength. (R) The value of sin $\theta/(\lambda_{ph}/\lambda_p)$ for different excitation wavelengths. All the data collapse toward the constant line sin $\theta/(\lambda_{ph}/\lambda_p) = 1$.

much faster than the phonon polaritons. Therefore, the propagating 1D plasmon, a dynamic charge density wave, excites the Cherenkov radiation of phonon polariton wake in hBN, which is analogous to a superluminal charged particle that generates Cherenkov radiation of light.[20,21] A schematic diagram of plasmons launching Cherenkov phonon polaritons is shown in Figure 1A. The emitted phonon polaritons are then probed and mapped by a scanning metallic atomic force microscope (AFM) tip. Note that the period of phonon polariton fringes extracted near the nanowire is twice that of the period extracted near the hBN edge (see Supporting Information S3) and is equal to the phonon polariton wavelength $\lambda_{ph}$. Figure 1C presents a representative infrared nanoimage of an SNW/hBN heterostructure at 6.55 $\mu$m excitation, and prominent phonon polaritons are observed. Interestingly, a nonzero angle between the phonon polariton wavefronts and the SNW shows up, and consequently the phonon polariton wavefronts form wakes. This can be understood quantitatively using Cherenkov physics, which is discussed later in more detail.

To confirm that the Cherenkov phonon polariton wakes are indeed launched by propagating longitudinal plasmons, we systematically investigated phonon polariton generation under different excitation polarizations. Previous studies have shown that plasmons of different modes in SNW can be excited by light with different polarization directions:[18] parallel polarization can excite longitudinal plasmon modes with periodically distributed charges along the nanowire, whereas perpendicular polarization will produce transverse plasmon modes with local charges distributed uniformly on the two sides of the nanowire. If the Cherenkov phonon polariton wakes are indeed launched by longitudinal plasmons, one should observe the wakes only when parallel-polarized light is illuminated on the nanowire. Experimentally, we rotated the laser polarization from near parallel ($\alpha \approx 0°$, Figure 2A) to perpendicular ($\alpha = 90°$, Figure 2D) relative to the nanowire while keeping the incident laser beam always normal to the


https://dx.doi.org/10.1021/acs.nanolett.0c00419
Nano Lett. 2020, 20, 2770–2777

nanowire and investigated the excitation of phonon polaritons. As expected, the orientation of the excited wavefronts shows a large distinction for the two polarizations: for polarization parallel to the nanowire, the excited phonon polariton wavefronts feature a hallmark V-shaped pattern of Cherenkov radiation, whereas for perpendicular polarization, the excited wavefronts are simply parallel to the nanowire and much weaker. The numerical simulation results in Figure 2B ($\alpha = 0°$) and Figure 2E ($\alpha = 90°$) illustrate this phenomenon more clearly.

The polarization-dependent Cherenkov radiation of phonon polaritons can be well understood by considering different plasmon modes in the nanowire. For polarization parallel to the nanowire ($\alpha = 0°$), plasmons are excited at the end of the nanowire and propagate longitudinally along the nanowire with a delayed phase at position away from the end. Because their phase velocity is faster than the phase velocity of phonon polaritons in hBN, such plasmons are always ahead of the phonon polaritons that they emit, generating Cherenkov V-shaped wave patterns around the nanowire. For polarization perpendicular to the nanowire ($\alpha = 90°$), transverse local plasmons with uniform phase along the nanowire are excited. These local plasmons act as trivial launchers and produce phonon polariton wavefronts parallel to the nanowire. Figure 2C,F presents the simulated corresponding longitudinal and transverse plasmon modes on the SNW. For parallel polarization, the phase evolution of plasmons and phonon polaritons along the nanowire displays the same speed. The coexistence of phonon polariton wakes and propagating longitudinal plasmons as well as the consistency in their phase evolution unambiguously confirms that Cherenkov wakes are emitted by propagating longitudinal plasmons. Experimental results for more excitation polarizations can be found in Supporting Information S4, showing that the Cherenkov radiation of phonon polaritons can be gradually turned on or off by continuously rotating the excitation polarization angle.

The Cherenkov radiation direction is controlled by the ratio of the phase velocities between the 2D phonon polaritons and the 1D plasmons. A longitudinal 1D plasmon is a running wave along the nanowire with a phase velocity $v_p = \lambda_p\omega_0/2\pi$ and a phase profile $\phi = 2\pi x/\lambda_p - \omega_0 t$, where $\omega_0$ is the excitation frequency. As shown in Figure 2A−C, the plasmons excite coherent phonon polaritons, which constructively interfere and create wakes with an angle $\theta$. The angle of the wakes can be derived by imposing the condition that the propagation phase shift ($2\pi\Delta x/\lambda_p$) between two points on the nanowire separated by a distance $\Delta x$ is exactly compensated by the phase shift ($2\pi\Delta x \sin\theta/\lambda_{ph}$) between phonon polariton wakes propagating out of those points. This condition yields

$$\sin\theta = \frac{\lambda_{ph}}{\lambda_p} = \frac{v_{ph}}{v_p} \quad (1)$$

where $v_{ph} = \lambda_{ph}\,\omega_0/2\pi$ is the phase velocity of the phonon polaritons. Note that to generate Cherenkov phonon polaritons, the condition $v_p > v_{ph}$ needs to be satisfied.

We would like to point out that hBN provides a particularly suitable platform to study Cherenkov physics. First, it holds high-quality and long-lifetime phonon polaritons due to the absence of electronic losses.[13] Second, the phase velocity of the phonon polaritons is tunable in a wide range by changing the excitation in the spectral range from transverse optical (TO) to longitudinal optical (LO) phonon frequencies;[13,15] on the other hand, the phase velocity of the plasmons in the SNW varies very slowly with the excitation wavelength. Thus, according to eq 1, the angle $\theta$ of the wakes is excitation-dependent, leading to in situ tunable Cherenkov radiation.

Next, we illustrate that the Cherenkov radiation direction is tunable by varying the excitation wavelengths. Figure 3A−D shows the experimental Cherenkov radiation of phonon polaritons in a 63 nm-thick hBN flake with excitation wavelength $\lambda_0$ changing from 6.45 to 6.60 $\mu$m (more data on a wider range of excitation wavelengths can be found in Supporting Information S5). The fringe period of phonon polaritons increases significantly from Figure 3A to Figure 3D. Additionally, the orientation of the phonon polariton fringes also varies, indicating a change in the Cherenkov radiation angle. The Cherenkov radiation at different excitations is also simulated using finite element analysis, the results of which are shown in Figure 3E−H. The simulated Cherenkov profiles match quite well with the experimental observations. Both the experiment and the simulation clearly reveal that the emission direction of the Cherenkov phonon polaritons can be controlled by varying the excitation wavelength. Figure 3I−N shows the plasmon oscillations along the SNW with excitation wavelength changing from 6.30 to 6.60 $\mu$m. Plasmon wavelength $\lambda_p$ is equal to twice the period of plasmon fringes along the SNW.

To quantitatively examine the Cherenkov radiation, we extracted the phonon polariton wavelengths $\lambda_{ph}$, plasmon wavelengths $\lambda_p$, and Cherenkov angle $\theta$ (see Supporting Information S9 for the determination of $\theta$) both experimentally and numerically for a series of excitation wavelengths. Figure 3O presents the experimental (red circles) and numerical (blue line) results for phonon polariton wavelengths. In the spectral region from 6.40 to 6.75 $\mu$m, a small variation in the excitation wavelength leads to a significant change in the phonon polariton wavelength from 0.2 to 1.0 $\mu$m. On the other hand, the change in the plasmon wavelength $\lambda_p$ is relatively small within 15%, as shown in Figure 3P. We note that the plasmon wavelength $\lambda_p$ can sometimes even exceed the free-space photon wavelength $\lambda_0$ (gray dashed line), implying a plasmon phase velocity faster than the speed of light $c$.[19] Figure 3Q displays the evolution of the Cherenkov angle $\theta$ from 2° at 6.40 $\mu$m excitation to 8° at 6.75 $\mu$m excitation. The Cherenkov angle and the phonon polariton wavelength have similar dependence on the excitation wavelength, which implies the dominant role of the phonon polariton wavelength in determining the Cherenkov angle $\theta$ in SNW/hBN heterostructures.

Continuing with verifying the Cherenkov angle predicted by eq 1, we compared the sine value of the angle $\theta$ with the ratio of the two wavelengths $\lambda_{ph}/\lambda_p$. Figure 3R plots $\sin\theta/(\lambda_{ph}/\lambda_p)$ for different excitation wavelengths. We found that all data collapse toward the constant line $\sin\theta/(\lambda_{ph}/\lambda_p) = 1$. In other words, $\sin\theta$ is exactly equal to the phase velocity of phonon polaritons $v_{ph}$ divided by the phase velocity of plasmons $v_p$, indicating that the observed emission direction of phonon polaritons is well described by Cherenkov physics.

We further show that the Cherenkov radiation angle is also tunable by changing the hBN flake thickness. Owing to the unique properties of 2D hyperbolic phonon polaritons, the phase velocity and wavelength of phonon polariton scale linearly with the hBN thickness $d$.[13,15] Therefore, we can deduce a simple relation between the Cherenkov angle and the


https://dx.doi.org/10.1021/acs.nanolett.0c00419
Nano Lett. 2020, 20, 2770−2777

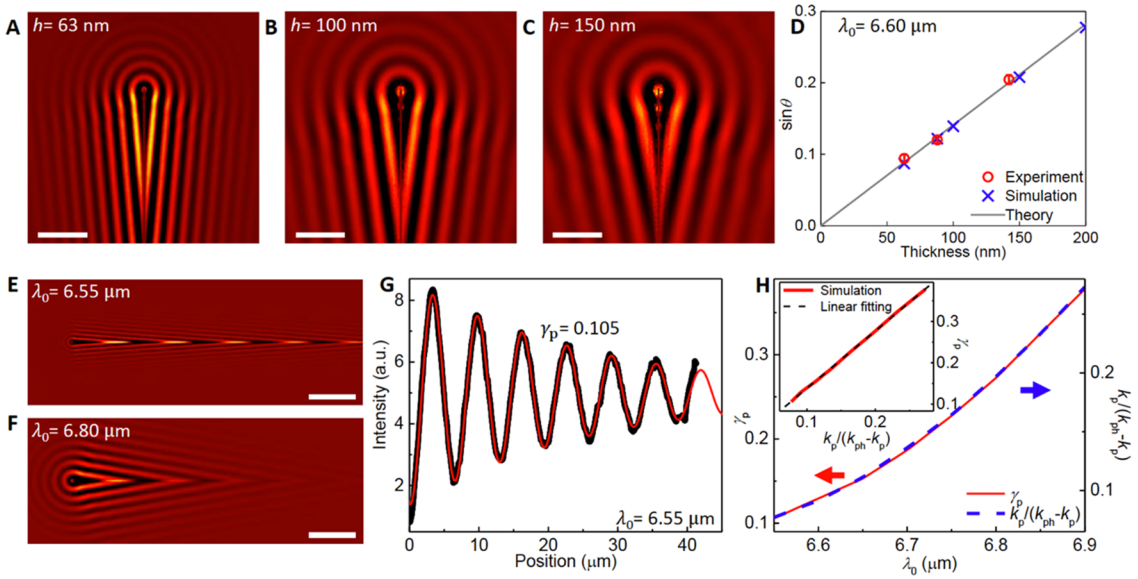


**Figure 4.** Thickness-dependent Cherenkov radiation and Cherenkov radiation-induced damping of 1D plasmons. (A−C) Numerical simulations of Cherenkov phonon polaritons in hBN with thickness of 63 nm (A), 100 nm (B), and 150 nm (C) at 6.60 $\mu$m excitation. (D) Experimentally (red circles) and numerically (blue crosses) obtained dependence of the Cherenkov angle on the hBN thickness. All the data match well with sin $\theta \propto d$ (gray line). (E,F) The decay of the simulated plasmons and phonon polaritons at two representative excitation wavelengths $\lambda_0$ = 6.55 $\mu$m (E) and 6.80 $\mu$m (F). Scale bars: 5 $\mu$m. (G) Line profile of damping of plasmon oscillations along the silver nanowire extracted from (E); the damping of plasmons is due to the Cherenkov radiation loss and a damping ratio $\gamma_p$ = 0.105 is extracted. (H) The extracted values of the plasmon damping ratio $\gamma_p$ and $k_p/(k_{ph} - k_p)$ as a function of the excitation wavelength. The inset shows $\gamma_p \propto k_p/(k_{ph} - k_p)$.

hBN thickness for a given excitation, sin $\theta \propto d$ (details in Supporting Information S10). Figure 4A−C shows the simulation results for hBN with a thickness range from 63 to 150 nm at 6.60 $\mu$m excitation. Both the experimental and numerical results match well with this relation, as shown in Figure 4D.

The emission direction can also be understood from the view of momentum matching. Along the nanowire, translational symmetry protects the conservation of momentum. The steering of the radiated phonon polaritons is ruled by such momentum conservation, that is, $k_p = k_{ph}$ sin $\theta$, where $k$ is the wave vector. Note that this is a special case of Snell's law at grazing incidence.

Momentum matching also controls the radiation rate of Cherenkov phonon polaritons. Plasmons excite and transfer energy and momentum to Cherenkov phonon polaritons. As a result, the plasmons lose energy, leading to a prominent decay in plasmon amplitude along the nanowire. Accordingly, the plasmon-excited phonon polaritons also show a decay along the nanowire with the same rate. The decay rate is largely determined by the Cherenkov radiation rate, considering that the Cherenkov radiation is the main decay channel of plasmons in the strong coupling region. Figure 4E,F presents the decay of the simulated plasmons and phonon polaritons at two representative excitation wavelengths $\lambda_0$ = 6.55 and 6.80 $\mu$m for a 63 nm thick hBN. The phonon polaritons show a lower decay rate at the excitation of 6.55 $\mu$m and a higher decay rate at 6.80 $\mu$m, reflecting a higher radiation rate at 6.80 $\mu$m than that at 6.55 $\mu$m. Figure 4G shows a representative plasmon damping profile along the SNW at excitation wavelength $\lambda_0$ = 6.55 $\mu$m. The quantitative decay rate can be extracted by fitting the oscillating profile of plasmons along the nanowire with an exponential decay form $e^{-2\pi\gamma_p x/\lambda_p} \sin(2\pi x/\lambda_p)$, where $x$ is the distance to the terminal of the nanowire and $\gamma_p$ is the damping ratio of plasmons. Figure 4H shows a dramatic growth of $\gamma_p$ with increasing wavelength. We attribute the growth of $\gamma_p$ to the increase of coupling strength between the 1D plasmons and the phonon polaritons. When the excitation wavelength increases, both the magnitude and the direction of the phonon polariton momentum approach those of the plasmon momentum. Therefore, the coupling between plasmons and phonon polaritons increases, which makes it easier for plasmons to transfer energy and momentum to phonon polaritons and leads to a higher Cherenkov radiation rate. A phenomenological relation between the relative momentum mismatch $(k_{ph} - k_p)/k_p$ and the plasmon damping ratio $\gamma_p$ is found over a spectral range from 6.55 to 6.90 $\mu$m

$$\gamma_p \propto \frac{k_p}{k_{ph} - k_p} \tag{2}$$

The damping ratio is inversely proportional to the relative momentum mismatch (inset of Figure 4H), which reveals a unique Cherenkov coupling between 1D plasmon polaritons and 2D phonon polaritons. This relation makes intuitive sense in terms of that the energy conversion from plasmons to phonon polaritons becomes more difficult and the plasmon damping ratio decreases accordingly when the momentum mismatch increases. Further theoretical studies need to be carried out to quantitatively describe the radiation rate of the Cherenkov phonon polaritons.

To conclude, we report the observation of Cherenkov radiation of phonon polaritons in a heterostructure of SNW/hBN, where phonon polariton wakes are emitted by 1D propagating plasmons with a phase velocity greater than that of phonon polaritons. Moreover, the observed Cherenkov radiation of phonon polaritons is tunable in both the radiation direction and radiation rate by varying the excitation frequency or changing the hBN thickness. Our observation represents the first example of Cherenkov-type coupling between 1D plasmon


https://dx.doi.org/10.1021/acs.nanolett.0c00419
Nano Lett. 2020, 20, 2770−2777

polaritons and 2D phonon polaritons in low-dimensional material heterostructures and provides a new avenue to launch 2D phonon polaritons and control their propagation at a deep subwavelength scale. The results provide deep insight into the interactions between polaritons of different dimensionality and hold great potential for novel polaritonic and nanophotonic devices and circuits based on low-dimensional material heterostructures.

## METHODS

**Near-Field Infrared Nanoimaging.** A home-built SNOM composed of a Bruker Innova AFM and a Daylight Solution quantum cascade laser (QCL) was used for near-field infrared nanoimaging. A mid-infrared light (1370−1610 $cm^{-1}$) generated by the QCL laser was focused onto the apex of a conductive AFM tip. The enhanced optical field at the tip apex interacted with the sample underneath the tip. The scattered light, carrying the local optical information of the sample, was collected by an MCT detector (KLD-0.1-J1, Kolmar) placed in the far field. Near-field optical images with spatial resolution better than 20 nm can be achieved with sharp AFM tips. Such near-field infrared images were recorded simultaneously with the topography information during our measurements. The polarization of infrared light was tuned using wire grid polarizers.

**Numerical Simulation.** Numerical simulations were conducted using the 3D wave optics module of the commercial software package COMSOL. In all simulations, the electric field component normal to the surface of the sample ($E_z$) was monitored. For Figure 2C,F and Figure 4E,F, to detect the plasmon electric field distribution on the SNW the electric field monitor was 100 nm above the hBN slab, whereas the distance was equal to 50 nm for all the other simulations. More simulation details can be found in Supporting Information S1 and S2.

## ASSOCIATED CONTENT

### Supporting Information

The Supporting Information is available free of charge at https://pubs.acs.org/doi/10.1021/acs.nanolett.0c00419.

(1) Numerical simulation, (2) infrared permittivity of hBN, (3) edge-reflected phonon polaritons and nanowire-launched phonon polaritons, (4) detailed dependence of Cherenkov phonon polaritons on excitation polarization, (5) detailed steering of Cherenkov phonon polaritons by varying the excitation wavelength, (6) excitation wavelength dependence of Cherenkov phonon polaritons in sample 2, (7) quantitative analysis of the Cherenkov behavior in sample 2, (8) simulated Cherenkov phonon polaritons in sample 2, (9) precise measurement of Cherenkov angle $\theta$ by 2D fast Fourier transform filtering, (10) derivation of linear relationship between Cherenkov angle $\theta$ and thickness of hBN (PDF)

## AUTHOR INFORMATION


### Corresponding Author

**Zhiwen Shi** − *Key Laboratory of Artificial Structures and Quantum Control (Ministry of Education), Shenyang National Laboratory for Materials Science, School of Physics and Astronomy, Shanghai Jiao Tong University, Shanghai 200240, China; Collaborative Innovation Center of Advanced Microstructures, Nanjing 210093, China;* orcid.org/0000-0002-3928-2960; Email: zwshi@sjtu.edu.cn

### Authors

**Yiran Zhang** − *Key Laboratory of Artificial Structures and Quantum Control (Ministry of Education), Shenyang National Laboratory for Materials Science, School of Physics and Astronomy, Shanghai Jiao Tong University, Shanghai 200240, China; Collaborative Innovation Center of Advanced Microstructures, Nanjing 210093, China;* orcid.org/0000-0002-8477-0074

**Cheng Hu** − *Key Laboratory of Artificial Structures and Quantum Control (Ministry of Education), Shenyang National Laboratory for Materials Science, School of Physics and Astronomy, Shanghai Jiao Tong University, Shanghai 200240, China; Collaborative Innovation Center of Advanced Microstructures, Nanjing 210093, China*

**Bosai Lyu** − *Key Laboratory of Artificial Structures and Quantum Control (Ministry of Education), Shenyang National Laboratory for Materials Science, School of Physics and Astronomy, Shanghai Jiao Tong University, Shanghai 200240, China; Collaborative Innovation Center of Advanced Microstructures, Nanjing 210093, China;* orcid.org/0000-0001-8044-5509

**Hongyuan Li** − *Key Laboratory of Artificial Structures and Quantum Control (Ministry of Education), Shenyang National Laboratory for Materials Science, School of Physics and Astronomy, Shanghai Jiao Tong University, Shanghai 200240, China; Collaborative Innovation Center of Advanced Microstructures, Nanjing 210093, China;* orcid.org/0000-0001-9119-5592

**Zhe Ying** − *Key Laboratory of Artificial Structures and Quantum Control (Ministry of Education), Shenyang National Laboratory for Materials Science, School of Physics and Astronomy, Shanghai Jiao Tong University, Shanghai 200240, China; Collaborative Innovation Center of Advanced Microstructures, Nanjing 210093, China*

**Lele Wang** − *Key Laboratory of Artificial Structures and Quantum Control (Ministry of Education), Shenyang National Laboratory for Materials Science, School of Physics and Astronomy, Shanghai Jiao Tong University, Shanghai 200240, China; Collaborative Innovation Center of Advanced Microstructures, Nanjing 210093, China*

**Aolin Deng** − *Key Laboratory of Artificial Structures and Quantum Control (Ministry of Education), Shenyang National Laboratory for Materials Science, School of Physics and Astronomy, Shanghai Jiao Tong University, Shanghai 200240, China; Collaborative Innovation Center of Advanced Microstructures, Nanjing 210093, China*

**Xingdong Luo** − *Key Laboratory of Artificial Structures and Quantum Control (Ministry of Education), Shenyang National Laboratory for Materials Science, School of Physics and Astronomy, Shanghai Jiao Tong University, Shanghai 200240, China; Collaborative Innovation Center of Advanced Microstructures, Nanjing 210093, China*

**Qiang Gao** − *Key Laboratory of Artificial Structures and Quantum Control (Ministry of Education), Shenyang National Laboratory for Materials Science, School of Physics and Astronomy, Shanghai Jiao Tong University, Shanghai 200240, China; Collaborative Innovation Center of Advanced Microstructures, Nanjing 210093, China*

**Jiajun Chen** − *Key Laboratory of Artificial Structures and Quantum Control (Ministry of Education), Shenyang National*




https://dx.doi.org/10.1021/acs.nanolett.0c00419
Nano Lett. 2020, 20, 2770−2777

*Laboratory for Materials Science, School of Physics and Astronomy, Shanghai Jiao Tong University, Shanghai 200240, China; Collaborative Innovation Center of Advanced Microstructures, Nanjing 210093, China*

**Jing Du** − *Key Laboratory of Artificial Structures and Quantum Control (Ministry of Education), Shenyang National Laboratory for Materials Science, School of Physics and Astronomy, Shanghai Jiao Tong University, Shanghai 200240, China; Collaborative Innovation Center of Advanced Microstructures, Nanjing 210093, China*

**Peiyue Shen** − *Key Laboratory of Artificial Structures and Quantum Control (Ministry of Education), Shenyang National Laboratory for Materials Science, School of Physics and Astronomy, Shanghai Jiao Tong University, Shanghai 200240, China; Collaborative Innovation Center of Advanced Microstructures, Nanjing 210093, China*

**Kenji Watanabe** − *National Institute for Materials Science, Tsukuba 305-0044, Japan;* orcid.org/0000-0003-3701-8119

**Takashi Taniguchi** − *National Institute for Materials Science, Tsukuba 305-0044, Japan;* orcid.org/0000-0002-1467-3105

**Ji-Hun Kang** − *Department of Optical Engineering, Kongju National University, Cheonan 31080, Korea;* orcid.org/0000-0002-2201-1689

**Feng Wang** − *Department of Physics, University of California at Berkeley, Berkeley, California 94720, United States; Materials Science Division, Lawrence Berkeley National Laboratory, Berkeley, California 94720, United States; Kavli Energy NanoSciences Institute, University of California, Berkeley and the Lawrence Berkeley National Laboratory, Berkeley, California 94720, United States*

**Yueheng Zhang** − *Key Laboratory of Artificial Structures and Quantum Control (Ministry of Education), Shenyang National Laboratory for Materials Science, School of Physics and Astronomy, Shanghai Jiao Tong University, Shanghai 200240, China; Collaborative Innovation Center of Advanced Microstructures, Nanjing 210093, China*

Complete contact information is available at: https://pubs.acs.org/10.1021/acs.nanolett.0c00419

### Author Contributions

Z.S. and Y.Z. conceived this project. Y.Z., B.L., Z.Y., L.W., X.L., and Q.G. prepared the nanowire heterostructure samples. Y.Z., C.H., B.L., and A.D. performed the near-field infrared measurements. C.H. carried out the numerical simulations. K.W. and T.T. provided the hBN crystals. Y.Z., C.H., B.L., H.L., J.-H. K., F.W., and Z.S. analyzed the data. All authors discussed the results and contributed to writing the manuscript.

### Author Contributions

○Y.Z. and C.H. contributed equally to this work.

### Notes

The authors declare no competing financial interest.

## ■ ACKNOWLEDGMENTS

We thank Prof. Fangwei Ye for helpful discussions. This work is supported by the National Key Research and Development Program of China (2016YFA0302001) and the National Natural Science Foundation of China (11774224 and 11574204). Z.S. acknowledges support from the National Thousand Youth Talents Plan, the Shanghai Thousand Talents Plan and the Program for Professor of Special Appointment (Eastern Scholar) at Shanghai Institutions of Higher Learning. K.W. and T.T. acknowledge support from the Elemental Strategy Initiative conducted by the MEXT, Japan, A3 Foresight by JSPS and the CREST (JPMJCR15F3), JST.

## ■ ABBREVIATIONS

2D, two-dimensional; hBN, hexagonal boron nitride; 1D, one-dimensional; SNW, silver nanowire; SNOM, scanning near-field optical microscopy; AFM, atomic force microscope; TO, transverse optical; LO, longitudinal optical

## ■ REFERENCES

(1) Yankowitz, M.; Xue, J.; Cormode, D.; Sanchez-Yamagishi, J. D.; Watanabe, K.; Taniguchi, T.; Jarillo-Herrero, P.; Jacquod, P.; LeRoy, B. J. Emergence of superlattice Dirac points in graphene on hexagonal boron nitride. *Nat. Phys.* **2012**, *8* (5), 382−386.

(2) Ponomarenko, L. A.; Gorbachev, R. V.; Yu, G. L.; Elias, D. C.; Jalil, R.; Patel, A. A.; Mishchenko, A.; Mayorov, A. S.; Woods, C. R.; Wallbank, J. R.; Mucha-Kruczynski, M.; Piot, B. A.; Potemski, M.; Grigorieva, I. V.; Novoselov, K. S.; Guinea, F.; Fal'ko, V. I.; Geim, A. K. Cloning of Dirac fermions in graphene superlattices. *Nature* **2013**, *497* (7451), 594−597.

(3) Dean, C. R.; Wang, L.; Maher, P.; Forsythe, C.; Ghahari, F.; Gao, Y.; Katoch, J.; Ishigami, M.; Moon, P.; Koshino, M.; Taniguchi, T.; Watanabe, K.; Shepard, K. L.; Hone, J.; Kim, P. Hofstadter's butterfly and the fractal quantum Hall effect in moiré superlattices. *Nature* **2013**, *497*, 598.

(4) Hunt, B.; Sanchez-Yamagishi, J. D.; Young, A. F.; Yankowitz, M.; LeRoy, B. J.; Watanabe, K.; Taniguchi, T.; Moon, P.; Koshino, M.; Jarillo-Herrero, P.; Ashoori, R. C. Massive Dirac Fermions and Hofstadter Butterfly in a van der Waals Heterostructure. *Science* **2013**, *340* (6139), 1427−1430.

(5) Yang, W.; Chen, G.; Shi, Z.; Liu, C.-C.; Zhang, L.; Xie, G.; Cheng, M.; Wang, D.; Yang, R.; Shi, D.; Watanabe, K.; Taniguchi, T.; Yao, Y.; Zhang, Y.; Zhang, G. Epitaxial growth of single-domain graphene on hexagonal boron nitride. *Nat. Mater.* **2013**, *12* (9), 792−797.

(6) Chen, G. R.; Jiang, L. L.; Wu, S.; Lyu, B.; Li, H. Y.; Chittari, B. L.; Watanabe, K.; Taniguchi, T.; Shi, Z. W.; Jung, J.; Zhang, Y. B.; Wang, F. Evidence of a gate-tunable Mott insulator in a trilayer graphene moire superlattice. *Nat. Phys.* **2019**, *15* (3), 237−241.

(7) Cao, Y.; Fatemi, V.; Demir, A.; Fang, S.; Tomarken, S. L.; Luo, J. Y.; Sanchez-Yamagishi, J. D.; Watanabe, K.; Taniguchi, T.; Kaxiras, E.; Ashoori, R. C.; Jarillo-Herrero, P. Correlated insulator behaviour at half-filling in magic-angle graphene superlattices. *Nature* **2018**, *556* (7699), 80.

(8) Cao, Y.; Fatemi, V.; Fang, S.; Watanabe, K.; Taniguchi, T.; Kaxiras, E.; Jarillo-Herrero, P. Unconventional superconductivity in magic-angle graphene superlattices. *Nature* **2018**, *556* (7699), 43.

(9) Jin, C.; Regan, E. C.; Yan, A.; Iqbal Bakti Utama, M.; Wang, D.; Zhao, S.; Qin, Y.; Yang, S.; Zheng, Z.; Shi, S.; Watanabe, K.; Taniguchi, T.; Tongay, S.; Zettl, A.; Wang, F. Observation of moiré excitons in WSe2/WS2 heterostructure superlattices. *Nature* **2019**, *567*, 76−80.

(10) Tran, K.; Moody, G.; Wu, F.; Lu, X.; Choi, J.; Kim, K.; Rai, A.; Sanchez, D. A.; Quan, J.; Singh, A.; Embley, J.; Zepeda, A.; Campbell, M.; Autry, T.; Taniguchi, T.; Watanabe, K.; Lu, N.; Banerjee, S. K.; Silverman, K. L.; Kim, S.; Tutuc, E.; Yang, L.; MacDonald, A. H.; Li, X. Jiamin Quan, Akshay Singh, Jacob Embley, André Zepeda, Marshall Campbell, Travis Autry, Takashi Taniguchi, Kenji Watanabe, Nanshu Lu, Sanjay K. Banerjee, Kevin L. Silverman, Suenne Kim, Emanuel Tutuc, Li Yang, Allan H. MacDonald & Xiaoqin Li Evidence for moiré excitons in van der Waals heterostructures. *Nature* **2019**, *567*, 71−75.

(11) Seyler, K. L.; Rivera, P.; Yu, H.; Wilson, N. P.; Ray, E. L.; Mandrus, D. G.; Yan, J.; Yao, W.; Xu, X. Signatures of moiré-trapped

valley excitons in MoSe2/WSe2 heterobilayers. *Nature* **2019**, *567*, 66−70.
(12) Chen, J.; Badioli, M.; Alonso-Gonzalez, P.; Thongrattanasiri, S.; Huth, F.; Osmond, J.; Spasenovic, M.; Centeno, A.; Pesquera, A.; Godignon, P.; Zurutuza Elorza, A.; Camara, N.; de Abajo, F. J. G.; Hillenbrand, R.; Koppens, F. H. L. Optical nano-imaging of gate-tunable graphene plasmons. *Nature* **2012**, *487* (7405), 77.
(13) Dai, S.; Fei, Z.; Ma, Q.; Rodin, A. S.; Wagner, M.; McLeod, A. S.; Liu, M. K.; Gannett, W.; Regan, W.; Watanabe, K.; Taniguchi, T.; Thiemens, M.; Dominguez, G.; Neto, A. H. C.; Zettl, A.; Keilmann, F.; Jarillo-Herrero, P.; Fogler, M. M.; Basov, D. N. Tunable phonon polaritons in atomically thin van der Waals crystals of boron nitride. *Science* **2014**, *343* (6175), 1125−1129.
(14) Shi, Z.; Hong, X.; Bechtel, H. A.; Zeng, B.; Martin, M. C.; Watanabe, K.; Taniguchi, T.; Shen, Y. R.; Wang, F. Observation of a Luttinger-liquid plasmon in metallic single-walled carbon nanotubes. *Nat. Photonics* **2015**, *9* (8), 515−519.
(15) Shi, Z.; Bechtel, H. A.; Berweger, S.; Sun, Y.; Zeng, B.; Jin, C.; Chang, H.; Martin, M. C.; Raschke, M. B.; Wang, F. Amplitude- and phase-resolved nanospectral imaging of phonon polaritons in hexagonal boron nitride. *ACS Photonics* **2015**, *2* (7), 790−796.
(16) Fei, Z.; Rodin, A. S.; Andreev, G. O.; Bao, W.; McLeod, A. S.; Wagner, M.; Zhang, L. M.; Zhao, Z.; Thiemens, M.; Dominguez, G.; Fogler, M. M.; Neto, A. H. C.; Lau, C. N.; Keilmann, F.; Basov, D. N. Gate-tuning of graphene plasmons revealed by infrared nano-imaging. *Nature* **2012**, *487* (7405), 82−85.
(17) Ju, L.; Geng, B.; Horng, J.; Girit, C.; Martin, M.; Hao, Z.; Bechtel, H. A.; Liang, X.; Zettl, A.; Shen, Y. R.; Wang, F. Graphene plasmonics for tunable terahertz metamaterials. *Nat. Nanotechnol.* **2011**, *6* (10), 630−634.
(18) Wei, H.; Li, Z.; Tian, X.; Wang, Z.; Cong, F.; Liu, N.; Zhang, S.; Nordlander, P.; Halas, N. J.; Xu, H. Quantum dot-based local field imaging reveals plasmon-based interferometric logic in silver nanowire networks. *Nano Lett.* **2011**, *11* (2), 471−475.
(19) Joshi, T.; Kang, J.-H.; Jiang, L.; Wang, S.; Tarigo, T.; Lyu, T.; Kahn, S.; Shi, Z.; Shen, Y.-R.; Crommie, M. F.; Wang, F. Coupled one-dimensional plasmons and two-dimensional phonon polaritons in hybrid silver nanowire/silicon carbide structures. *Nano Lett.* **2017**, *17* (6), 3662−3667.
(20) Cherenkov, P. A. Visible emission of clean liquids by action of $\gamma$ radiation. *Doklady Akademii Nauk SSSR* **1934**, *2*, 451.
(21) Frank, I.; Tamm, I. Coherent visible radiation of fast electrons passing through matter. *Compt. Rend. Acad. Sci. USSR* **1937**, *14*, 109.
(22) Liu, F.; Xiao, L.; Ye, Y.; Wang, M.; Cui, K.; Feng, X.; Zhang, W.; Huang, Y. Integrated Cherenkov radiation emitter eliminating the electron velocity threshold. *Nat. Photonics* **2017**, *11*, 289.
(23) Xi, S.; Chen, H.; Jiang, T.; Ran, L.; Huangfu, J.; Wu, B.-I.; Kong, J. A.; Chen, M. Experimental Verification of Reversed Cherenkov Radiation in Left-Handed Metamaterial. *Phys. Rev. Lett.* **2009**, *103* (19), 194801.
(24) Genevet, P.; Wintz, D.; Ambrosio, A.; She, A.; Blanchard, R.; Capasso, F. Controlled steering of Cherenkov surface plasmon wakes with a one-dimensional metamaterial. *Nat. Nanotechnol.* **2015**, *10* (9), 804−809.
(25) Adamo, G.; MacDonald, K. F.; Fu, Y. H.; Wang, C. M.; Tsai, D. P.; García de Abajo, F. J.; Zheludev, N. I. Light Well: A Tunable Free-Electron Light Source on a Chip. *Phys. Rev. Lett.* **2009**, *103* (11), 113901.
(26) Lin, X.; Easo, S.; Shen, Y. C.; Chen, H. S.; Zhang, B. L.; Joannopoulos, J. D.; Soljacic, M.; Kaminer, I. Controlling Cherenkov angles with resonance transition radiation. *Nat. Phys.* **2018**, *14* (8), 816.


https://dx.doi.org/10.1021/acs.nanolett.0c00419
*Nano Lett.* 2020, 20, 2770−2777